ISSN 1070-3284, Russian Journal of Coordination Chemistry, 2017, Vol. 43, No. 1, pp. 63–72. © Pleiades Publishing, Ltd., 2017.

Synthesis, Crystal Structures, and Properties of Copper(II) Dicarboxylate Complexes with [Bis(2-Pyridylcarbonyl)amido][1]

J. Q. Xu, Y. Q. Zheng*, and W. Xu

Center of Applied Solid State Chemistry Research, Ningbo University, Ningbo, 315211 P.R. China

**e-mail: yqzhengmc@163.com*

Received October 28, 2015

Abstract—Four new complexes, $[Cu_2(Bpca)_2(L^1)(H_2O)_2] \cdot 3H_2O$ (**I**), $[Cu_2(Bpca)_2(L^2)(H_2O)_2]$ (**II**), $[Cu_2(Bpca)_2(L^3)] \cdot 2H_2O$ (**III**), $[Cu_2(Bpca)_2(L^1)(H_2O)] \cdot 2H_2O$ (**IV**) (Bpca = bis(2-pyridylcarbonyl)amido, H_2L^1 = glutaric acid, H_2L^2 = adipic acid, H_2L^3 = suberic acid, H_2L^4 = azelaic acid) have been synthesized and characterized by single-crystal X-ray diffraction methods (CIF files CCDC nos. 1432836 (**I**), 1432835 (**II**), 817411 (**III**), and 817412 (**IV**)), elemental analyses, IR spectra. Structural analyses reveal that compounds **I**, **II**, and **IV** have similar structures $[Cu(Bpca)]^+$ units bridged by dicarboxylate forming dinuclear units, whereas the dinuclear of compound **III** are edge-shared through two carboxylate oxygen atoms of different suberate anions. Hydrogen bonds are response for the supramolecular assembly of compounds **I** to **IV**. The temperature-dependent magnetic property of **III** was also investigated in the temperature range of 2 to 300 K, and the magnetic behaviour suggests weak antiferromagnetic coupling exchange.

Keywords: Cu(II) complex, Bpca, crystal structure, magnetic properties

DOI: 10.1134/S1070328417010092

INTRODUCTION

The construction of supramolecular system and crystal engineering have been received much attention not only for their intriguing structural topologies but also for their potential applications in biotechnology, catalysis, sorption, luminescence and magnetism etc. [1–10]. Recently, more and more researchers have focused on the rational design of supermolecule with desired structural and magnetism. One of the useful synthetic strategies consists in the use of multifunctional ligands and target metal ions. As we know, 2,4,6-tris(2-pyridyl)-1,3,5-triazine (Tptz) has attracted much attention in coordination chemistry because of its multiple coordination sites, large π system and potential ability to function as a bridging ligand. However, copper(II) and Rh(II) are able to promote the hydrolysis of Tptz in soft conditions yielding the bis(2-pyridylcarbonyl)amido (Bpca) and picolinamide (2-pyridylformamide) [11–14], while 2,4,6-triaryltriazines are quite stable toward hydrolysis and concentrated mineral acid with 150°C required for hydrolytic reaction. The hydrolytic reaction occurs via nucleophilic attack at the triazine ring by OH^- or H_2O [11, 15].

The hydrolysate product (Bpca) would seem to be a perfect bridging ligand because two oxygen atoms and three nitrogen atoms could be coplanar with the coordination metal cations [16–20]. So the ligand is widely used to construct homo- and heterometallic complexes. As an ongoing part of our systematic investigation on reaction of Cu^{2+}, Tptz, or different dicarboxylic acid in methanol–water at room temperature afforded different hydrolytic products [21, 22]. In this context, we describe the synthesis and crystal structures of four dicarboxylate-bridged [bis(2-pyridylcarbonyl)amido]copper(II) complexes, $[Cu_2(Bpca)_2(L^1)(H_2O)_2] \cdot 3H_2O$ (**I**), $[Cu_2(Bpca)_2(L^2)(H_2O)_2]$ (**II**), $[Cu_2(Bpca)_2(L^3)] \cdot H_2O$ (**III**), $[Cu_2(Bpca)_2(L^1)(H_2O)] \cdot 2H_2O$ (**IV**).

EXPERIMENTAL

Material and physical methods. All chemicals of reagent grade were commercially available and used without further purification. The FT-IR spectrums were recorded from KBr pellets in the range of 4000–400 cm^{-1} on a Shimadzu FTIR-8900 spectrometer. Thermogravimetric (TG) measurements were carried out under a flow of nitrogen gas from room temperature to 700°C with a heating rate of 10 K/min using a Seiko Exstar 6300 TG/DTA apparatus. The single crystal data was collected on a Rigaku R-Axis Rapid X-ray diffractometer using a Mo target (λ = 0.71073 Å). Powder X-ray diffraction measurements

[1] The article is published in the original.

were carried out with a Bruker D8 Focus X-ray diffractometer using a Cu target (λ = 1.54056 Å) and a Ni filter at room temperature with the range of 2θ between 5° and 50° to check the phase purity. The C, H, and N microanalyses were performed with a Perkin-Elmer 2400II elemental analyzer. The variable susceptibilities were measured using a Quantum Design SQUID magnetometer (Quantum Design Model MPMS-7) in the temperature range of 2–300 K with an applied field of 1 kOe.

Synthesis of I. Dropwise addition of 1 M NaOH (2.0 mL) to a stirred aqueous solution of $CuCl_2 \cdot 2H_2O$ (0.171 g, 1.0 mmol) gave a blue precipitate, which was separated by centrifugation and washed with doubly distilled water five times. The fresh blue precipitate was transferred to a stirred solution of 0.312 g (1.0 mmol) Tptz and 0.132 g (1.0 mmol) glutaric acid in 20 mL CH_3OH–H_2O (1 : 1 v/v). The mixture solution was further stirred for half an hour and then filtered, the filtrate allowed to stand at room temperature and blue plate crystals were grown by slow evaporation for over five days (the yield (54%) based on the initial $CuCl_2 \cdot 2H_2O$). The product phase purity was checked according to the experimental PXRD pattern with the one simulated on the basis of the single crystal data.

For $C_{29}H_{32}N_6O_{13}Cu_2$

anal. calcd., %:	C, 43.56;	H, 3.50;	N, 10.50.
Found, %:	C, 43.63;	H, 3.56;	N, 10.42.

IR (KBr; ν, cm^{-1}): 3419 m, 3088 w, 1717 s, 1566 m, 1364 s, 1290 w, 1157 w, 1101 w, 1026 w, 762 m, 702 m, 631 m.

Synthesis of II was similar to that of **I**, except that glutaric acid was replaced by adipic acid. Blue plate crystals were grown by slow evaporation for over five days (the yield (48%) based on the initial $CuCl_2 \cdot 2H_2O$). The product phase purity was checked according to the experimental PXRD pattern with the one simulated on the basis of the single crystal data.

For $C_{30}H_{28}N_6O_{10}Cu_2$

anal. calcd., %:	C, 47.43;	H, 3.72;	N, 11.06.
Found, %:	C, 47.49;	H, 3.65;	N, 11.02.

IR (KBr; ν, cm^{-1}): 3492 m, 3124 w, 2932 w, 2864 w, 1713 s, 1582 m, 1360 s, 1292 w, 1094 w, 1049 w, 1026 w, 762 m, 706 m, 625 m.

Synthesis of III was similar to that of **I**, except that glutaric acid was used instead of suberic acid. Blue plate crystals were grown by slow evaporation for over five days (the yield (53%) based on the initial $CuCl_2 \cdot 2H_2O$). The product phase purity was checked according to the experimental PXRD pattern with the one simulated on the basis of the single crystal data.

For $C_{32}H_{32}N_6O_{10}Cu_2$

anal. calcd., %:	C, 48.79;	H, 4.09;	N, 10.67.
Found, %:	C, 48.86;	H, 4.15;	N, 10.62.

IR (KBr; ν, cm^{-1}): 3572 w, 3487 w, 3116 w, 2939 w, 2847 w, 1707 s, 1603 m, 1358(s), 1294 m, 1092 w, 1028 w, 760 m, 708 m, 631 w.

Synthesis of IV was analogous to that of **I** with glutaric acid used in place of azelaic acid. Blue plate crystals were grown by slow evaporation for over five days (the yield (61%) based on the initial $CuCl_2 \cdot 2H_2O$). The product phase purity was checked according to the experimental PXRD pattern with the one simulated on the basis of the single crystal data.

For $C_{33}H_{36}N_6O_{11}Cu_2$

anal. calcd., %:	C, 48.35;	H, 4.43;	N, 10.25.
Found, %:	C, 48.39;	H, 4.38;	N, 10.32.

IR (KBr; ν, cm^{-1}): 3516 w, 3450 w, 3074 w, 2930 w, 2853 w, 1713 s, 1601 m, 1362 s, 1292 s, 1090 w, 1026 w, 802 w, 760 m, 704 w, 622 m.

X-ray crystallography. Suitable single crystals of **I**–**IV** were selected under a polarizing microscope and fixed with epoxy cement on the respective fine glass fibres, which were then mounted on a Rigaku R-Axis Rapid diffractometer with graphite-monochromated MoK_α radiation (λ = 0.71073 Å) for cell determination and subsequent data collection. The data were corrected for *Lp* and absorption effects. The SHELXS-97 [23] and SHELXL-97 [24] programs were used for structure solution and refinement. The structures were solved by direct methods and all non-hydrogen atoms to be located in the subsequent difference Fourier syntheses. After several cycles of refinement, all hydrogen atoms associated with carbon atoms were geometrically generated, and the rest of the hydrogen atoms were located from the successive difference Fourier syntheses, while the water H atoms of two split oxygen atoms O(12), O(13) and two oxygen atoms O(9) and O(10) in **I** could not be positioned reliably and were omitted from a difference Fourier map. Finally, the full-matrix least-squares technique was used to refine all non-hydrogen atoms with anisotropic displacement parameters and the hydrogen atoms with isotropic displacement parameters set to 1.2 times those of their carrier atoms. Detailed information about the data collection and structure determination is summarized in Table 1. Selected distances and bond angles are given in Table 2. Geometric parameters of hydrogen bonds are listed in Table 3.

Crystallographic data for the compounds deposited with the Cambridge Crystallographic Data Center

Table 1. Summary of crystal data, data collection, structure solution and refinement details for **I**–**IV**

Parameter	Value			
	I	**II**	**III**	**IV**
Formula weight	795.65	759.68	787.72	819.78
Description	Platelet	Platelet	Platelet	Block
Crystal size, mm	0.38 × 0.15 × 0.11	0.38 × 0.29 × 0.15	0.35 × 0.22 × 012	0.21 × 0.15 × 0.11
Temperature	293(2)	293(2)	293(2)	293(2)
Crystal system	Monoclinic	Monoclinic	Monoclinic	Triclinic
Space group	$P\,2_1/n$	$P\,2_1/c$	$P\,2_1/n$	$P\bar{1}$
a, Å	18.021(4)	8.356(2)	9.038(2)	10.456(2)
b, Å	7.214(2)	13.528(3)	13.367(3)	12.385(3)
c, Å	26.803(5)	15.480(5)	13.683(3)	14.670(3)
α, deg	90	90	90	110.40(3)
β, deg	109.46(3)	119.10(2)	94.27(3)	92.14(3)
γ, deg	90	90	90	103.66(3)
Volume, Å^3	3285.4(1)	1529.0(7)	1648.5(3)	1715.2(8)
Z	4	2	2	2
ρ_{calcd}, g cm^{-3}	1.600	1.650	1.587	1.310
$F(000)$	1608	776	808	844
μ, mm^{-1}	1.370	1.460	1.358	1.310
θ Range, deg	3.04–25.00	2.13–27.49	3.03–27.43	2.99–25.00
Reflections collected	24658	4533	15463	13543
Unique reflections (R_{int})	5778 (0.0506)	3495 (0.0283)	3726 (0.0299)	6013 (0.0453)
Data/restraints/parameters	4155/0/453	2949/0/217	3223/3/232	3354/9/469
Goodness of fit on F^2	1.162	1.028	1.084	1.106
R_1, wR_2 ($I \geq 2\sigma(I)$)*	0.0443, 0.1087	0.0320, 0.0813	0.0311, 0.0735	0.0496, 0.1040
R_1, wR_2 (all data)*	0.0801, 0.1606	0.0416, 0.0872	0.0400, 0.0812	0.1183, 0.1630
A, B values in weighting scheme**	0.0647, 7.6997	0.0428, 0.7883	0.0407, 0.8379	0.0493, 3.8892
$\Delta\rho_{max}/\Delta\rho_{min}$, e Å^{-3}	0.856/−1.025	0.527/−0.382	0.475/0.475	0.719/−1.140

* $wR_2 = [\Sigma w(F_o^2 - F_c^2)^2/\Sigma w(F_o^2)^2]^{1/2}$; ** $w = [\sigma^2(F_o^2) + (AP)^2 + BP]^{-1}$ with $P = (F_o^2 + 2F_c^2)/3$.

(CCDC nos. 1432836 (**I**), 1432835 (**II**), 817411 (**III**), and 817412 (**IV**); deposit@ccdc.cam.ac.uk or http://www.ccdc.cam.ac.uk).

RESULTS AND DISCUSSION

Single-crystal X-ray diffraction analysis reveals that compound **I** consists of dinuclear Cu(II) complex and lattice waters. As depicted in Fig. 1a, each Cu^{2+} cation is coordinated by three nitrogen of Bpca and one oxygen atom from glutarato ligand and an aqua ligand to form CuN_3O_2 square pyramid with the τ = 0.06 for Cu(1) and τ = 0.02 for Cu(2) (τ = 0 and 1 for ideal square pyramid and trigonal bipyramid, respectively) [25]. Three nitrogen atoms from Bpca ligand and one oxygen atom from glutarate anion define the basal plane. The distance from the basal plane of Cu(1) and Cu(2) are 0.164 and 0.150 Å, respectively. And the basal bond distances fall in region of 1.939(4)−2.021(4) Å, while the axial Cu(1)−O(9) and Cu(2)−O(1) bonds length are 2.336(4) and 2.270(4) Å, respectively (Table 2). The two adjacent square-pyramids are linked by glutarato to form the dinuclear copper(II) unit. As shown in Fig. 2a, the chain structure is formed in the [010] direction through two types of intermolecular hydrogen bonds, O(9)···O(6)$^{\#1}$ ($^{\#1}$ 1 − x, −y, −z); O(8)···O(10)$^{\#2}$ ($^{\#2}$ 1 − x, 1 − y, −z). The hydrogen bonds O(9)···O(3)$^{\#1}$ interchain assemble the 1D chains into 2D layers parallel to (101) as shown in Fig. 3a.

The compound **II** is similar to that of **I** consisting of $[Cu_2(Bpca)_2(L^2)]$. As illustrated in Fig. 1b, the Cu^{2+} cations are in a distorted square-pyramidal CuN_3O_2

Table 2. Selected distances (Å) and bond angles (deg) for **I***

Bond	*d*, Å	Bond	*d*, Å	Bond	*d*, Å
		I			
Cu(1)–O(5)	1.943(3)	Cu(1)–N(3)	2.021(4)	Cu(2)–N(4)	2.004(4)
Cu(1)–O(9)	2.336(4)	Cu(2)–O(7)	1.939(4)	Cu(2)–N(5)	1.940(4)
Cu(1)–N(1)	2.007(4)	Cu(2)–O(10)	2.270(4)	Cu(2)–N(6)	1.998(5)
Cu(1)–N(2)	1.940(4)				
		II			
Cu(1)–O(1)	2.302(2)	Cu(1)–N(1)	2.021(2)	Cu(1)–N(3)	2.007(2)
Cu(1)–O(4)	1.952(2)	Cu(1)–N(2)	1.950(2)		
		III			
Cu(1)–N(2)	1.936(2)	Cu(1)–N(1)	2.002(2)	Cu(1)–O(3)$^{\#1}$	2.364(1)
Cu(1)–O(3)	1.947(1)	Cu(1)–N(3)	2.004(2)		
		IV			
Cu(1)–O(3)	1.927(4)	Cu(1)–N(3)	2.020(6)	Cu(2)–N(4)	1.986(5)
Cu(1)–N(1)	2.004(5)	Cu(1)–O(5)	2.338(4)	Cu(2)–N(5)	1.920(5)
Cu(1)–N(2)	1.929(5)	Cu(2)–O(8)	1.903(5)	Cu(2)–N(6)	1.004(5)
Angle	ω, deg	Angle	ω, deg	Angle	ω, deg
		I			
N(2)Cu(1)O(5)	166.7(2)	N(1)Cu(1)N(3)	163.0(2)	N(5)Cu(2)N(6)	82.4(2)
N(2)Cu(1)N(1)	81.4(2)	N(1)Cu(1)O(9)	87.6(2)	N(5)Cu(2)N(4)	81.6(6)
N(2)Cu(1)N(3)	82.0(2)	N(3)Cu(1)O(9)	98.7(2)	N(5)Cu(2)O(10)	103.3(2)
N(2)Cu(1)O(9)	100.0(2)	O(7)Cu(2)N(5)	165.1(2)	N(6)Cu(2)N(4)	164.0(2)
O(5)Cu(1)N(1)	99.1(2)	O(7)Cu(2)N(6)	97.1(2)	N(6)Cu(2)O(10)	89.6(2)
O(5)Cu(1)N(3)	96.2(2)	O(7)Cu(2)N(4)	98.5(2)	N(4)Cu(2)O(10)	93.5(2)
O(5)Cu(1)O(9)	93.3(2)	O(7)Cu(2)O(10)	91.6(2)		
		II			
N(1)Cu(1)O(1)	91.1(1)	N2Cu(1)O(4)	171.9(2)	O(4)Cu(1)O(1)	89.6(1)
N2Cu(1)N(3)	80.9(1)	N(3)Cu(1)O(1)	97.2(2)	O(4)Cu(1)N(1)	98.7(1)
N(2)Cu(1)N(1)	81.6(1)	N(3)Cu(1)N(1)	161.6(1)	O(4)Cu(1)N(3)	97.8(1)
N(2)Cu(1)O(1)	98.5(1)				
		III			
N(1)Cu(1)N(3)	161.4(1)	N(2)Cu(1)O(3)	176.4(1)	O(3)Cu(1)N(1)	99.6(1)
N(1)Cu(1)O(3)$^{\#1}$	97.8(1)	N(2)Cu(1)O(3)$^{\#1}$	99.2(1)	O(3)Cu(1)N(3)	96.4(1)
N(2)Cu(1)N(1)	82.2(1)	N(3)Cu(1)O(3)$^{\#1}$	94.9(1)	O(3)Cu(1)O(3)$^{\#1}$	77.4(1)
N(2)Cu(1)N(3)	82.5(1)				
		IV			
N(1)Cu(1)N(3)	162.8(2)	N(2)Cu(1)O(5)	96.2(2)	N(4)Cu(2)N(6)	163.8(2)
N(1)Cu(1)N(2)	81.8(2)	N(3)Cu(1)O(3)	98.4(2)	N(4)Cu(2)O(8)	97.9(2)
N(1)Cu(1)O(3)	97.7(2)	N(3)Cu(1)O(5)	94.7(2)	N(5)Cu(2)N(6)	82.4(2)
N(1)Cu(1)O(5)	91.5(2)	O(3)Cu(1)O(5)	89.5(2)	N(5)Cu(2)O(8)	171.6(2)
N(2)Cu(1)N(3)	81.6(2)	N(4)Cu(2)N(5)	82.4(2)	N(6)Cu(2)O(8)	98.0(2)
N(2)Cu(1)O(3)	174.4(2)				

* Symmetry codes: $^{\#1}$ $-x, -y + 1, -z$ (for **III**).

Table 3. Geometric parameters of hydrogen bonds of **I**–**IV***

D–H···A	Distance, Å			Angle DHA, deg
	D–H	H···A	D···A	
		I		
O(9)–H(91)···O(3)$^{\#1}$	0.83	2.17	2.992(6)	173
O(9)–H(92)···O(6)$^{\#2}$	0.82	1.96	2.772(5)	169
O(10)–H(101)···O(11)$^{\#3}$	0.84	1.93	2.772(3)	180
O(10)–H(102)···O(8)$^{\#2}$	0.82	1.96	2.792(4)	179
O(11)–H(111)···O(2)	0.83	2.16	2.991(6)	180
O(11)–H(112)···O(1)$^{\#4}$	0.83	2.10	2.934(5)	180
* Symmetry codes: $^{\#1}$ $x + 1/2, -y + 1/2, z + 1/2$; $^{\#2}$ $x, y - 1, z$; $^{\#3}$ $-x + 3/2, y - 1/2, -z + 1/2$, $^{\#4}$ $-x + 2, -y + 1, -z + 1$.				
		II		
O(1)–H(1*A*)···O(5)$^{\#1}$	0.85	1.89	2.729(3)	168
O(1)–H(1*B*)···O(3)$^{\#2}$	0.84	2.06	2.866(3)	162
* Symmetry codes: $^{\#1}$ $-x + 1, y + 1/2, -z + 3/2$; $^{\#2}$ $x, -y + 3/2, z + 1/2$.				
		III		
O(5)–H(5*A*)···O(2)	0.85	2.09	2.926(3)	166
O(5)–H(5*B*)···O(2)$^{\#2}$	0.85	1.99	2.825(2)	168
* Symmetry codes: $^{\#2}$ $x + 1/2, -y + 1/2, z + 1/2$.				
		IV		
O(5)–H(5*B*)···O(7)$^{\#1}$	0.87	2.01	162	2.844(7)
O(5)–H(5*A*)···O(2)$^{\#2}$	0.84	2.21	134	2.855(6)
O(5)–H(5*A*)···O(1)$^{\#2}$	0.84	2.45	147	3.185(7)
O(10)–H(10*B*)···O(6)$^{\#3}$	0.85	2.17	149	2.930(8)
O(10)–H(10*C*)···O(3)	0.83	2.12	171	2.942(7)
O(11)–H(11*B*)···O(9)$^{\#4}$	0.88	2.10	136	2.802(9)
O(11)–H(11*C*)···O(4)	0.85	2.00	173	2.842(8)
* Symmetry codes: $^{\#1}$ $-x, -y, -z$; $^{\#2}$ $-x, -y + 2, -z + 1$; $^{\#3}$ $-x, -y, -z$; $^{\#4}$ $x, y + 1, z$.				

coordination sphere with trigonality parameter τ of 0.17. The basal plane consists of three nitrogen atoms from Bpca ligand and one oxygen atom from adipate anion. Cation Cu^{2+} is lifted 0.130 Å above the mean plane fitted to the four atoms direction towards the apical oxygen atom O(1). The distance Cu(1)–O(1) (2.302(2) Å) is rather longer than those of Cu–N (1.950(2)–2.021(2) Å) and Cu–O (1.952(2) Å) (Table 2) which form the basal plane. The two adjacent square-pyramids are linked by adipate to form a structure of dinbuclear copper. Neighboring dinuclear units are linked together via O–H···O hydrogen bond between coordinated water and carbonyl oxygen atom (O(3)) of a Bpca constructing the 2D layers along the (100) direction (Fig. 2b). The adjacent 2D layers form a 3D structure by intermolecular hydrogen bonds O(1)–H(1*B*)···O(5) with O(1)···O(5) 2.729 Å and ∠O(1)–H(1*B*)···O5) 168° (Table 3, Fig. 3b).

Compound **III** consists of $[Cu_2(Bpca)_2(L^3)]$ and lattice waters. As show in Fig. 1c, each Cu^{2+} cation is coordinated by three nitrogens from Bpca and two oxygens from suberato ligand to complete a CuN_3O_2 square-pyramid. In contrast to **II**, the apical site is occupied by oxygen from carboxylate. The Cu–N bond lengths vary from 1.936(2) to 2.004(2) Å, while Cu–O bond distances is 1.947(1) and 2.364(1) Å. The coordination sphere of Cu^{2+} has a τ value of 0.25, which indicates that Cu^{2+} is a square pyramid. Furthermore, the (CuN_3O_2) coordinated polyhedral are edge-shared through two carboxylate oxygen atoms of different suberato ligands, and the roofs locate opposite directions with Cu···Cu 3.373(2) Å. The chain of dinuclears is bridged by suberate anions along [100] direction (Fig. 2c). The adjoining chains connect form a 3D structure (Fig. 4) by intermolecular hydrogen-

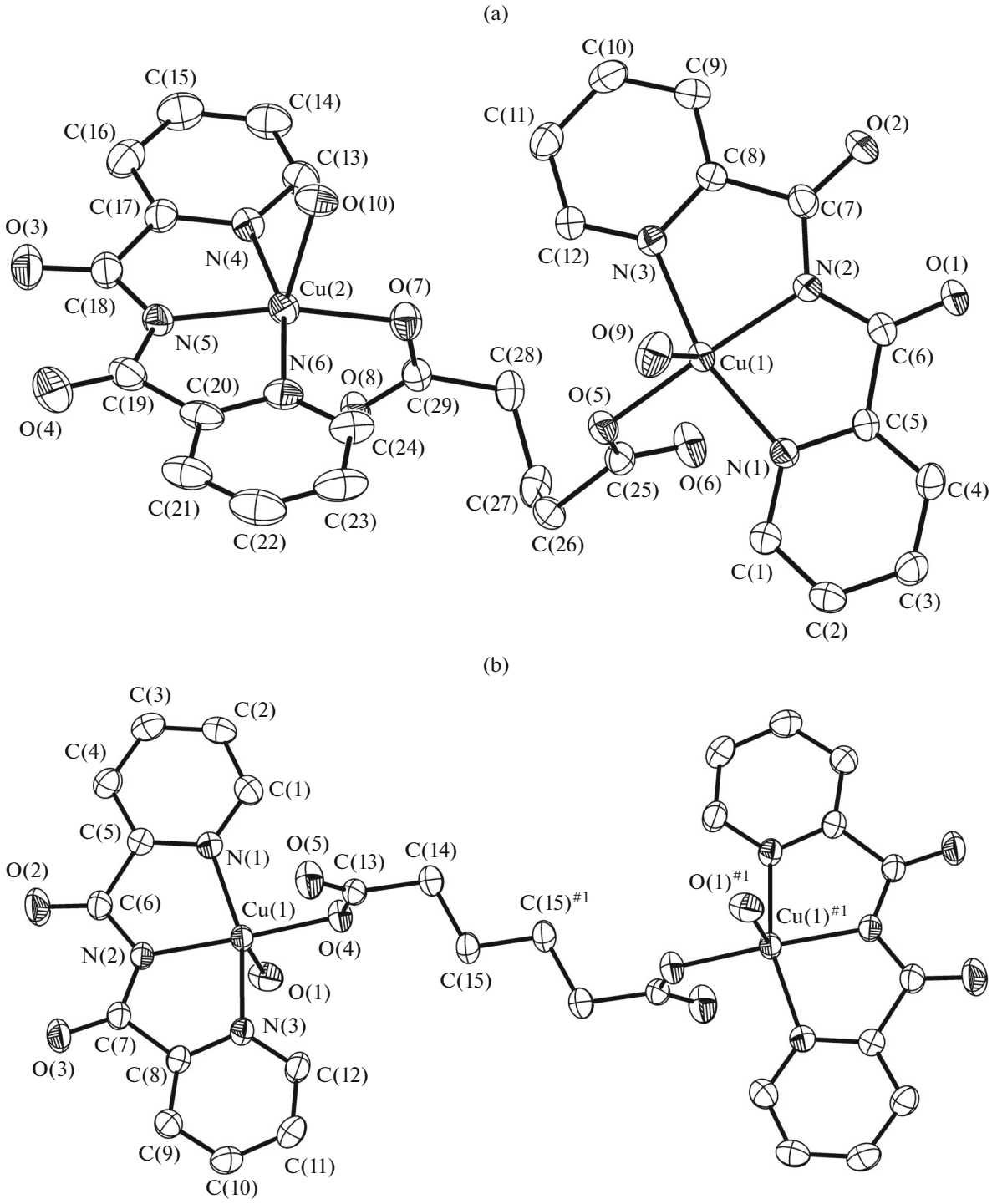

Fig. 1. Ortep view of the complexes: **I** (a), **II** (b), **III** (c), **IV** (d) with displacement ellipsoids (45% probability) and atomic labeling.

bonding with O(5)–H(5*A*)···O(2) and O(5)–H(5*B*)···O(4)$^{\#2}$ (Table 3).

The asymmetric unit of complex **IV** consists of distorted square-pyramidal CuN_3O_2 and tetragon CuN_3O_1 coordination sphere, respectively (Fig. 1d). The distorted square-pyramidal environment of Cu(1) has three N of a Bpca ligand, one oxygen atom from carboxylate and the other oxygen at the vertex of the pyramid from coordinated water. The basal bonds distances fall in the range of 1.927(4) to 2.020(6) Å, while the axial Cu(1)–O(5) bond length is 2.338(4) Å (Table 2). The quadrangular of Cu(2) is coordinated by three N of another Bpca, one O from carboxylate.

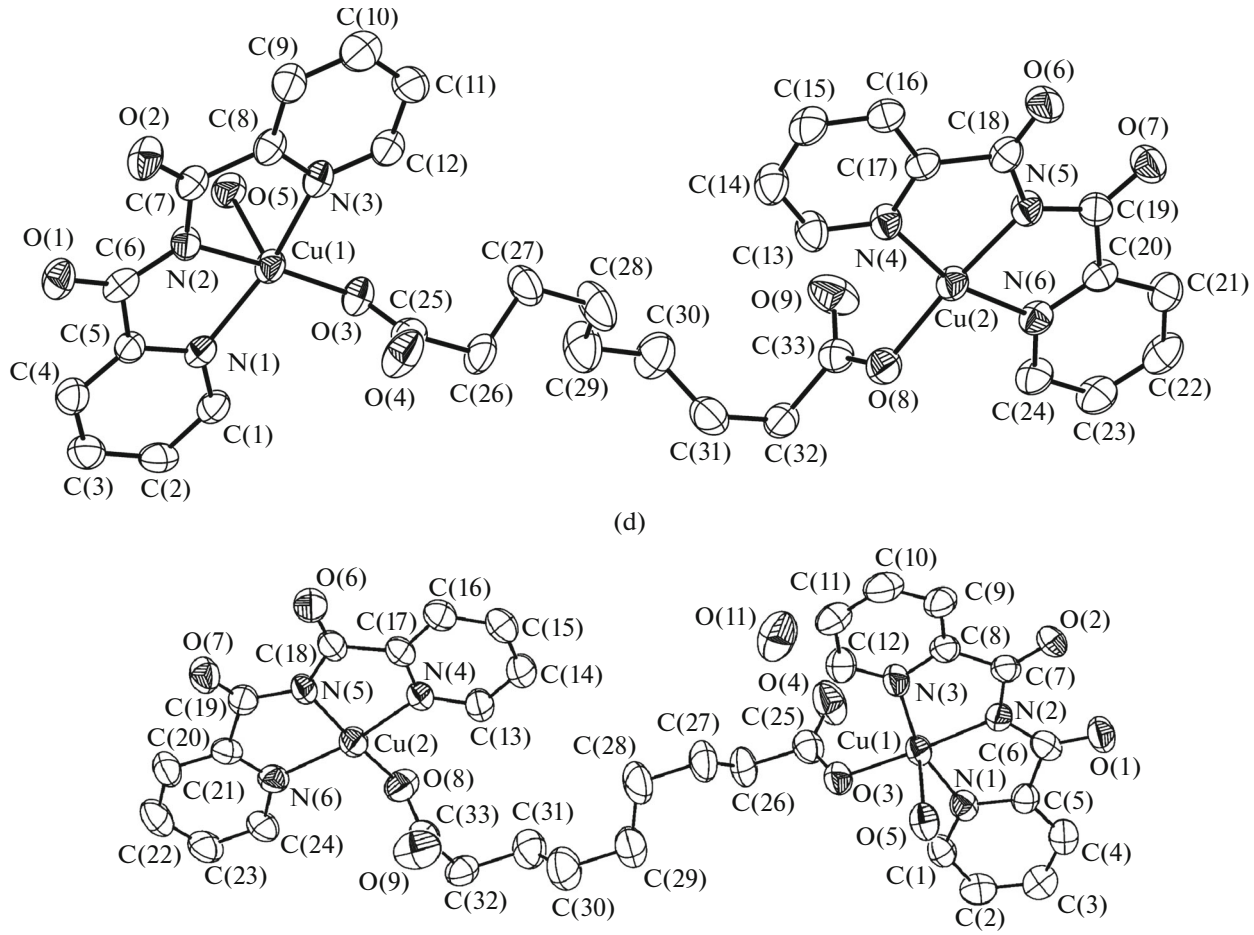

Fig. 1. (Contd.)

The Cu–N bond lengths are in the region of 1.920(5) to 1.994(5), as well as the Cu–O distance is 1.903(5). The distance from the basal plane of Cu(1) and Cu(2) are 0.094 and 0.045 Å, respectively. The azelato ligand links the square-pyramidal and tetragon, forming a dinuclear copper(II) structure. Four types of hydrogen bonds (O(5)–H(5*A*)···O(2)$^{\#3}$, O(5)–H(5*B*)···O(7)$^{\#2}$, O(11)–H(11*B*)···O(9)$^{\#5}$, and O(11)–H(11*C*)···O(4)) make a contribution to assemble 2D layers parallel to (100) direction (Fig. 3c).

We prepared four Cu(II) complexes based on aliphatic dicarboxylic acids (glutaric, adipic, suberic, and azelaic acid) with Bpca ligand. The results indicate that different dicarboxylic acids show significant effect on the final structures of **I**–**IV**. Compounds **I**–**III** crystallize in monoclinic space groups, while complex **IV** crystallizes in the triclinic space group $P\bar{1}$. All copper(II) atoms are in a distorted square-pyramidal CuN_3O_2 coordination sphere in addition to Cu(1) of complex **IV** presents quadrangular CuN_3O coordination sphere. In **I**, **II** and **IV**, dicarboxylate anions adopt the monodentate coordination mode linking $[Cu(Bpca)]^+$ ions to form a dinuclear $[Cu_2(Bpca)_2L(H_2O)_x]$. For **III**, the adjacent $[Cu(Bpca)]^+$ ions are linked by oxygen atoms from dicarboxylic anions forming edge-shared dinuclears, which linked by dicarboxylic anions to constitute 1D chain. Three compounds have been reported, which containing aliphatic dicarboxylic acids (oxalic acid [26], succinic acid [22] and sebacic acid [21]), and $[Cu(Bpca)]^+$ ions. All Cu^{2+} ions in these reported compounds present distorted square-pyramidal CuN_3O_2 and these compounds are 0D structure, which are different from compound **III** and **IV**.

The thermal behaviour of the compounds **I**–**IV** were studied. The TG curves of **I**–**IV** show two steps (Fig. 5). For **I**, the observed weight loss for the first step is 11.1% from 38 to 108°C, close to the calculate value (11.3%) for the loss of three lattice water molecules and two coordinated water molecules per formula unit, while the second weight loss is 64.8%, which is less than the calculated weight value of 72.9% for the removal of all organic components (glutarate and Bpca) from 284 to 700°C. The weight of the resi-

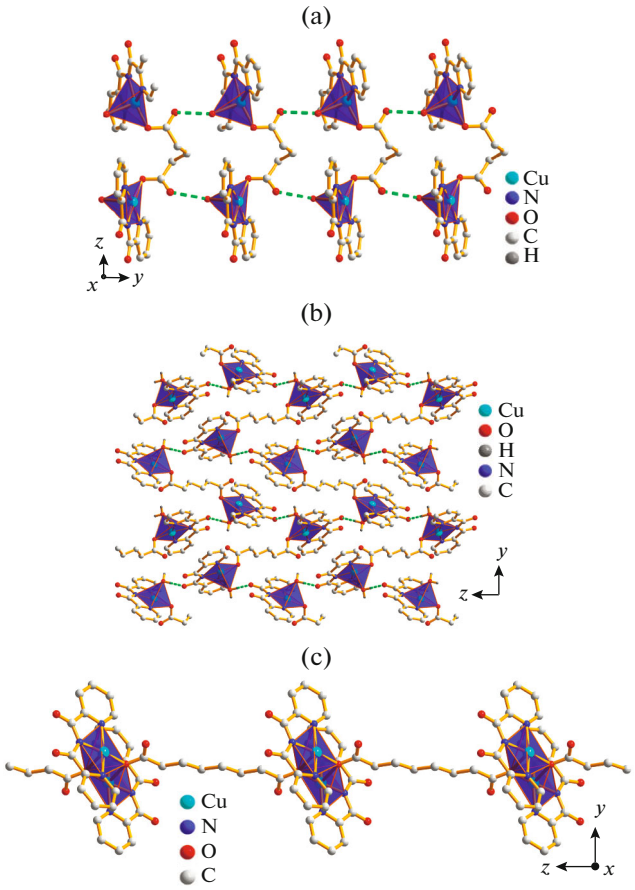

Fig. 2. View of the 1D chain structure **I** (a) and the 1D structures **II** (b) and **III** (c).

due remaining after heating at 700°C is 24.1%. And TG analysis suggests that dehydration of **II** starts at 109°C and terminates at 173°C, at these temperatures the observed weight loss of 5.4% corresponds well to the calculated value of 4.7% for two H_2O molecules per formula unit. The weight loss of 72.6% from 272–444°C is less than the calculated value 78.5% expected for Bpca and adipate. When further heated, the resulting intermediate loses weight very slowly. When the temperature reaches 700°C, the residual weight is 18.5%. For compound **III**, the first weight loss of 5.0% in the range 41–127°C, which agree well with liberation of two lattice water molecule per formula unit. The weight loss of 74.9% in the second step between 278–423°C is smaller than the value of 79.2% calculated for the decomposition of the organic ligands. The weight of the residue remaining at 700°C is 19.6%. The TG curve of **IV** indicated that the total weight loss of 6.5% over 57–115°C, which can be attributed to the loss of three lattice waters and one coordinated water molecule per formula unit (calcd. 6.6%). A single sharp mass loss of 76.1% occurred between 254 and 442°C is less than the value of 77.9%

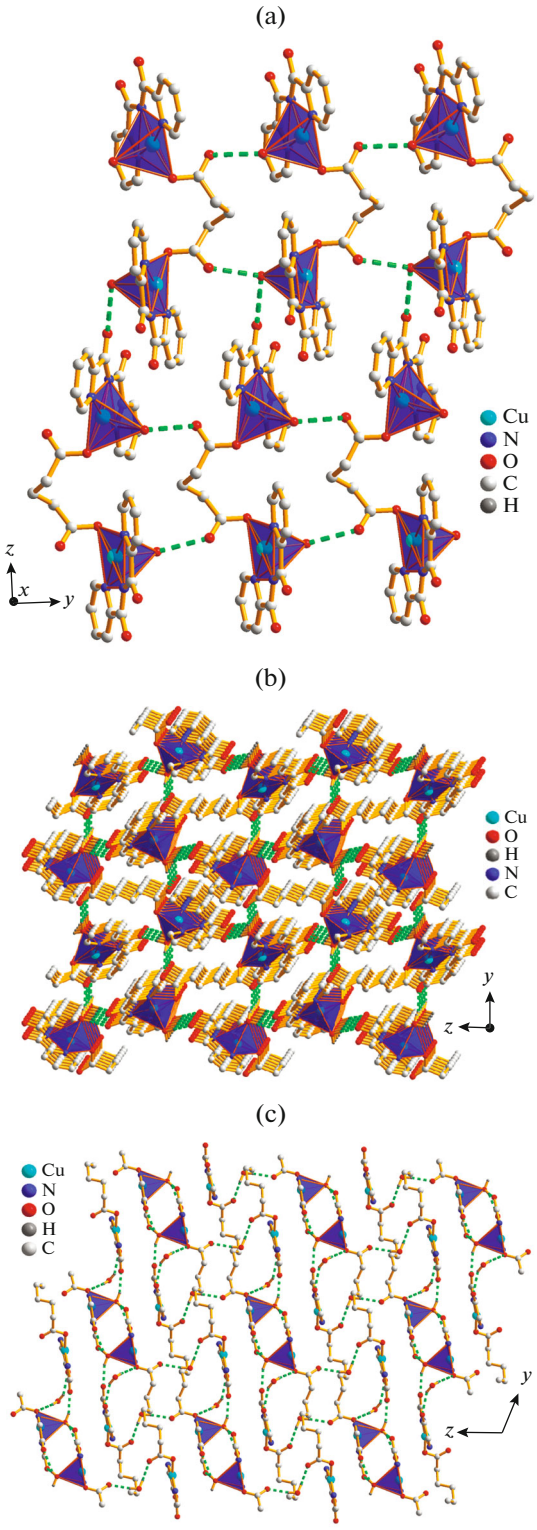

Fig. 3. View of the 2D layers parallel to (101) of **I** (a), **II** (b) and parallel to (100) of **IV** (c).

calculated for the decomposition of the organic ligands. The weight of residual solid product of thermal decomposition is 17.8%.

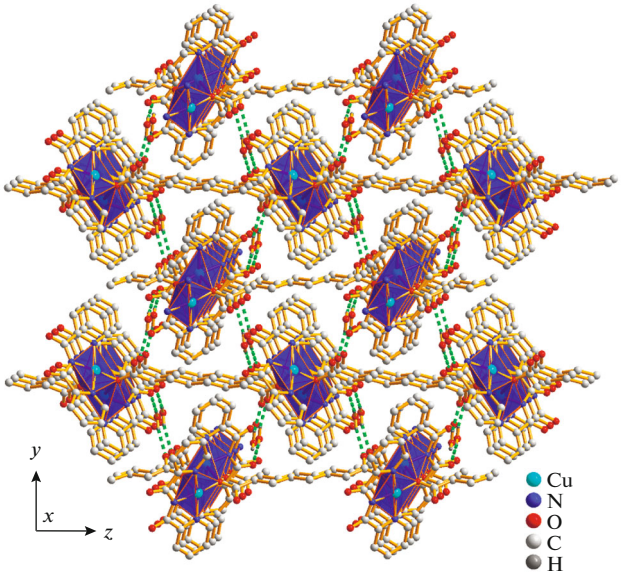

Fig. 4. View of the 3D structure of **III**.

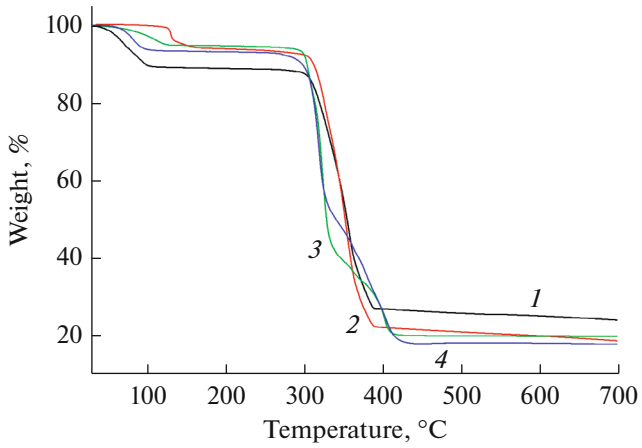

Fig. 5. TG curves for **I**–**IV**.

Temperature-dependent magnetic susceptibilities measurements for **III** were performed on the polycrystalline sample in the range 2–300 K in a fixed magnetic field 1 kOe, and the magnetic behaviours in the form of $\chi_m T$ and χ_m versus T were depicted in Fig. 6 (χ_m being the magnetic susceptibility per two Cu^{2+} ions). The value of $\chi_m T$ value at room temperature (0.66 $cm^3\ mol^{-1}\ K$) is lower than the spin-only value of 0.83 $cm^3\ mol^{-1}\ K$ expected for a dinuclear Cu^{2+} ion ($S = 1/2$) system with $g = 2.0$. With a decrease in temperature, the $\chi_m T$ increase to a maximal value of 0.78 $cm^3\ mol^{-1}\ K$ at 50 K. A further decrease in temperature causes sharply falling to the $\chi_m T$ value of 0.10 $cm^3\ mol^{-1}\ K$ at 2 K, suggesting an antiferromagnetic coupling between Cu^{2+} ions.

According to the crystal structure of **III**, the effective transmitting pathway of the magnetic coupling between Cu^{2+} ions can contribute to the carboxylate bridging ligand in *syn-anti* conformation mode Eq. (1) [27].

Due to the very weak magnetic interactions between ions, the expression is corrected using the molecular field approximation (Eq. (2)), to which the magnetic susceptibility data were fitted.

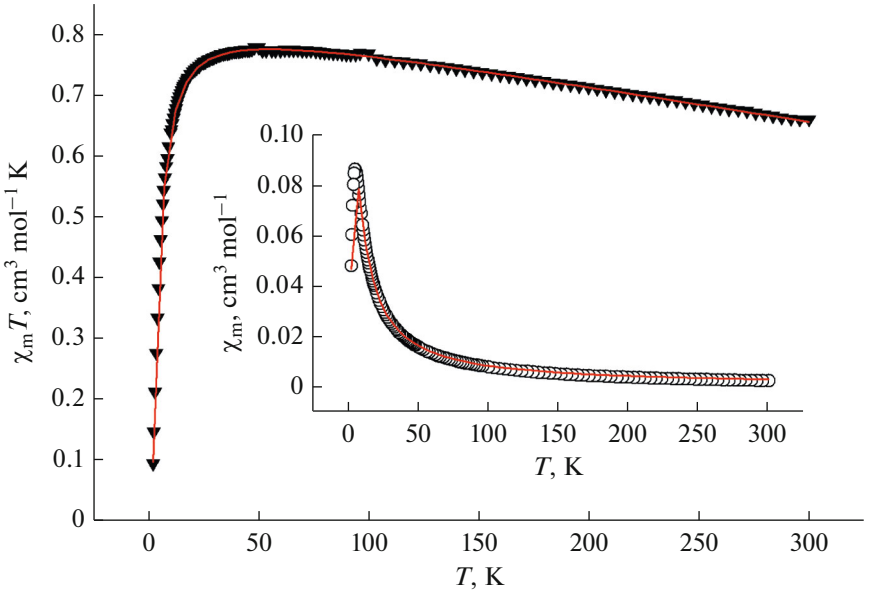

Fig. 6. χ_m and $\chi_m T$ vs T plots for complex **IV**. Solid lines represent the best fits.

$$\chi_m = (1-\rho)\frac{2N\beta^2 g^2}{3kT}\left[1+\frac{1}{3}\exp\left(-2J/kT\right)\right]^{-1} + 2\rho\left(\frac{N\beta^2 g_i^2}{4kT}\right) + N\alpha, \quad (1)$$

$$\chi'_m = \frac{\chi_m}{1-\chi_m(2zJ'/N\beta^2 g^2)}. \quad (2)$$

The best fit is obtained with values of $g = 2.115$, $J = -2.876\ cm^{-1}$, $zJ = -0.029\ cm^{-1}$, and $R = 1 \times 10^{-5}$ ($R = \sum[(\chi_m)_{obs} - (\chi_m)_{calc}]^2/[(\chi_m)_{obs}]^2$). The negative J and zJ' clearly indicates the existence of the antiferromagnetic coupling between adjacent Cu^{2+} ions, consistent with the magnetic behaviour illustrated by the $\chi_m T$ vs. T plot.

ACKNOWLEDGMENTS

This project was supported by the Non-Metallic Mineral Engineering Research Center of Zhejiang Province (no. ZD2015k05) and K.C. Wong Magna Fund in Ningbo University.

REFERENCES

1. Abdi, K., Hadadzadeh, H., Weil, M., and Rudbari, H.A., *Inorg. Chim. Acta*, 2014, vol. 416, p. 109.
2. Guo, J., Ma, J.F., Li, J.J., et al., *Cryst. Growth Des.*, 2012, vol. 12, p. 6074.
3. Jones, L.F., Kilner, C.A., Miranda, M.P.D., et al., *Angew. Chem. Int. Ed.*, 2007, vol. 46, p. 4073.
4. Adarsh, N.N. and Dastidar, P., *Chem. Soc. Rev.*, 2012, vol. 41, p. 3039.
5. Shu, Y.B., Xu, C., and Liu, W.S., *Eur. J. Inorg. Chem.*, 2013, vol. 21, p. 3592.
6. Tanaka, H., Kajiwara, T., Kaneko, Y., et al., *Polyhedron*, 2007, vol. 26, p. 2105.
7. Huang, H.C., Jupiter, D., Qiu, M., et al., *Biopolymers*, 2008, vol. 89, p. 210.
8. Lee, J.Y., Farha, O.K., Roberts, J., et al., *Chem. Soc. Rev.*, 2009, vol. 38, p. 1450.
9. Li, J.R., Kuppler, R.J., and Zhou, H.C., *Chem. Soc. Rev.*, 2009, vol. 38, p. 1477.
10. Allendorf, M.D., Bauer, C.A., Bhakta, R.K., and Houk, R.J.T., *Chem. Soc. Rev.*, 2009, vol. 38, p. 1330.
11. Lerner, E.I. and Lippard, S.J., *J. Am. Chem. Soc.*, 1976, vol. 98, p. 5397.
12. Lerner, E.I. and Lippard, S.J., *Inorg. Chem.*, 1997, vol. 16, p. 1546.
13. Paul, P., Tyagi, B., Bhadbhade, M.M., and Suresh, E., *J. Chem. Soc., Dalton Trans.*, 1997, p. 2273.
14. Paul, P., Tyagi, B., Bilakhiya, A.K., et al., *Inorg. Chem.*, 1998, vol. 37, p. 5733.
15. Faus, J., Julve, M., Amigo, J.M., and Debaerdemaeker, T., *J. Chem. Soc., Dalton, Trans.*, 1989, p. 1681.
16. Lu, Z.L., Lu, J., Huang, X.M., et al., *J. Mol. Struct.*, 2014, vol. 1064, p. 76.
17. Abd, K., Hadadzadeh, H., Weil, M., and Rudbari, H.A., *Inorg. Chim. Acta*, 2014, vol. 416, p. 109.
18. Kamiyama, A., Noguchi, T., Kajiwara, T., and Ito, T., *CrystEngComm*, 2003, vol. 5, p. 231.
19. Vangdal, B., Carranza, J., Lloret, F., et al., *Dalton Trans.*, 2002, p. 566.
20. Kaneko, Y., Kajiwara, T., Yamane, H., and Yamashita, M., *Polyhedron*, 2007, vol. 26 p. 2074.
21. Xu, W., Zhu, H.L., Lin, J.L., and Zheng, Y.Q., *J. Coord. Chem.*, 2013, vol. 66, p. 171.
22. Xu, W., Pan, W.J., and Zheng, Y.Q., *J. Coord. Chem.*, 2013, vol. 66, p. 4415.
23. Sheldrick, G.M., *SHELXL-97, Program for Crystal Structure Refinement*, Göttingen: Univ. of Göttingen, 1997.
24. Sheldrick, G.M., *SHELXS-97, Program for Crystal Structure Solution*, Göttingen: Univ. of Göttingen, 1997.
25. Addison, A.W., Rao, T.N., Reedijk, J., et al., *Dalton Trans.*, 1984, p. 1349.
26. Calatayud, M.L., Castro, I., Sletten, J., et al., *Inorg. Chim. Acta*, 2000, vol. 300, p. 846.
27. Kahn, O., *Molecular Magnetism*, Weinheim: VCH, 1993, p. 135.